Journal of Electrostatics 96 (2018) 16–22

Contents lists available at ScienceDirect

Journal of Electrostatics

journal homepage: www.elsevier.com/locate/elstat

Contact electrification and charge decay on polyester fibres: A KPFM study

Jun Yin, Bernard Nysten*

Institute of Condensed Matter and Nanosciences - Bio and Soft Matter, Université Catholique de Louvain, Croix Du Sud, 1/L7.04.02 - 1348, Louvain-la-Neuve, Belgium

ARTICLE INFO

Keywords:
Contact electrification
Charge decay
Polyester fibres
Kelvin probe force microscopy (KPFM)

ABSTRACT

Surface contact electrification experiments have been performed on insulating polyester fibres in contact with a conductive fibre using biased atomic force microscopy tips. With positive tip bias, charge spots have been deposited in a reproducible manner. The density of deposited charges on the fibre surface was observed by Kelvin probe force microscopy as a function of time, charging position and relative humidity. Two main charge dissipation mechanisms were identified with different importance depending on the relative humidity value.

1. Introduction

Contact electrification and electrostatic discharge (ESD) are known as serious risks in many domains. Antistatic fabrics are thus widely used in many applications, such as sophisticated microelectronic devices in electronic industry, in the chemical industry and in industries using filters [1,2]. In antistatic materials, the most widely used method consists in dispersing conductive fibres inside the highly resistive base fabrics. This method has the advantages to provide effective conductivity and long-term durability. The key is that the accumulated charges should be safely and quickly dissipated. However, nowadays the understanding of the mechanisms of charge generation and dissipation behaviours on surface and in bulk of insulating materials, especially the insulating fibres, is far from being completed [3,4].

Many efforts have been done to perform surface charging experiments on polymer materials at the macroscopic scale in order to understand these mechanisms [5–9]. In these works, surface charging was achieved by different techniques applied for different purposes, such as corona charging [6,10–12], electron beam [13–15], contact electrification (with or without friction) [16–20], etc. The charging mechanisms depend largely on the technique used for charging the surface, depending on the source of carriers. For example, X-rays and electron beams are used to trigger a number of reactions initiated by breaking covalent bonds and forming free-radicals and ions. Corona discharge is a powerful way to produce atmospheric ions, together with light and unstable chemicals such as ozone [21].

Kelvin probe force microscopy (KPFM) was first reported in 1991 [22] and is used to measure the distribution of surface potential and detecting charges on a wide range of materials, such as metals, semiconductors and insulating materials, under different experimental conditions [23–28]. Recently, KPFM has also been used to perform contact electrification experiments [19,28–36]. The use of biased AFM probes to induce charge electrification and to create electrostatic patterns on insulating films gain widespread interests. Some mechanisms have been proposed in the scope of KPFM results. An electrochemical charging mechanism with ionic charge carriers mediated by the field-adsorbed water meniscus on the biased probe was discussed by Knorr and co-workers, for dried amorphous polymer films, in particular hydrophobic polymer surfaces [30,37]. Belarni et al. attributed the charging to the generation of space charge polarization, which may arise from trap assisted tunnelling of electrons from the tip to defects in the dielectric [35]. Baytekin et al. obtained new insight into the charging mechanisms and demonstrated that contact charging phenomena derive from the microchemical and possibly micromechanical properties at and near the surface of the contacting polymers [33,38]. Regarding the charge dissipation mechanisms, the surface conductance and water absorption and desorption events have been proposed as the key parameters [21,34].

In this study, contact electrification experiments have been performed for the first time on the surface of insulating fibres by KPFM in order to investigate charge generation and dissipation mechanisms at the microscopic scale in antistatic felts. Contact charging studies previously reported in the literature were always realized on flat insulating film glued or spun directly on a metallic support, allowing a good contact between the sample and the electrode. One of the main challenge in the present study was to obtain a reliably electrical contact of the cylindrical polyester fibres presenting a rough surface with the back electrode. With biased AFM probes, charges were successfully deposited on the surface of polyester fibres in contact with a stainless steel conductive fibre. The deposited charges and charge dissipation were studied as a function of time, relative humidity, and distance between the charging point and the contact with the conductive fibre.

* Corresponding author.
E-mail addresses: yinjun5552@gmail.com (J. Yin), bernard.nysten@uclouvain.be (B. Nysten).

https://doi.org/10.1016/j.elstat.2018.09.002
Received 3 July 2018; Received in revised form 5 September 2018; Accepted 10 September 2018

2. Materials and methods

Two types of industrial fibres were used in this study: insulating polyester fibres and conductive stainless steel fibres. The brand name of the conductive stainless steel fibres is Bekinox fibres produced by the company Bekaert in Belgium. The fibres are commercially available and are used along with textile (polyester) fibres for manufacturing anti-static filters for filtering different kinds of powders. Both the stainless steel fibres and the polyester fibres were received from the company Sioen Nordifa (Belgium). The diameter of the stainless steel fibres varies between 7 and 13 μm, and that of polyester fibres varies between 10 and 20 μm. The fibres were stored under ambient conditions. Prior to the electrification experiments, the fibres were rinsed with distilled water and dried for 12 h in ambient air in order to remove contaminants from the surface.

KPFM experiments (one-pass mode) were performed using a Picoplus 5500 Atomic Force Microscope (Agilent Technologies) equipped with a scanner of maximum scanning area of 100 μm, with a MAC III AC module and an extender electronic module. Pointprobes probes coated with a layer of Pt/Ir on tip and detector sides were obtained from Nanosensors. The typical spring constant and resonance frequency of the cantilevers were 1.2–29 N m^{-1} and 75–260 kHz, respectively. The single-pass scan acquires topographical and surface potential images simultaneously [39].

On conductive surfaces, the measured surface potential refers to the surface contact potential due to the difference of work function between the sample and tip materials to which an applied potential may be added [40]. However, it is not so easy to interpret the signals measured on insulating surfaces by KPFM. In a working approximation, one may consider that charge densities which are constant on an area large enough to be resolved by KPFM are proportional to the measured surface potential. Under this assumption, the surface charge density σ located on the insulating surface can be approximated by a capacitor equation [30,33].

$$\sigma(x, y) = \varepsilon\varepsilon_0 V_{SP}(x, y)d^{-1} \quad (1)$$

with ε_0 the vacuum permittivity, ε the dielectric constant of the insulating material, V_{SP} the measured surface potential and d the average distance between the tip and the surface. This equation expresses the fact that the charge induced in the probe/electrode capacitor by the applied voltage has to match the charge on the insulator surface in order to nullify the electric field between the charge and the probe. Although the absolute value of charge density is still difficult to derive in these experiments on insulating surfaces, the charge density may safely be considered as being proportional to the measured surface potential.

Schemes of the experimental setups used for the biased probe electrification experiments are presented in Fig. 1. Fig. 1(a) shows the sample configuration where a single polyester fibre is in galvanic contact with a grounded conductive fibre, both glued on a AFM standard sample puck with insulating double-face adhesive tape. Fig. 1(b) shows the setup used to study the influence of the distance from the contact point with the conductive fibre. The different positions were identified as follows: P1 was the cross point of the polyester fibre and the conductive fibre, P2 was located 50 μm away from P1, P3 100 μm from P1, and P4 200 μm from P1. As mentioned in the introduction, the contact with the grounded electrode is crucial in contact electrification experiments on fibres. If the contact is bad, charges will accumulate on the side facing the conductive support rather than on the top surface [30]. Different setups were thus tested before using the one presented in Fig. 1 where the polyester fibre is in electrical contact with a grounded conductive fibre.

After mounting the fibres as depicted in Fig. 1, all the samples were put in the environmental chamber of the AFM during one night under controlled relative humidity to ensure full stabilization of the setup. Previous studies showed that the surface potential may have a strong dependence on relative humidity; a low relative humidity reduces the discharge rate [30]. In order to compare the results for different relative humidity (RH) values, different saturated salt solutions were used in the environmental chamber containing the sample: lithium chloride for 15% RH, potassium acetate for 25% RH, potassium carbonate for 46% RH and sodium chloride for 75% RH.

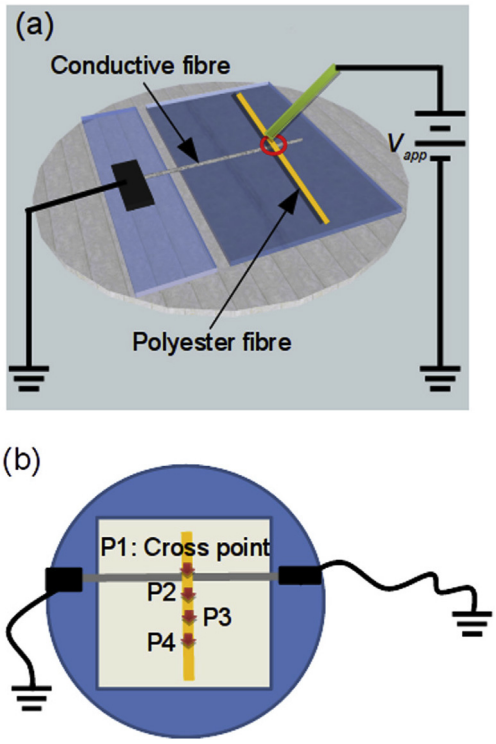

Fig. 1. Scheme of biased probe contact electrification experiments. (a) Sample configuration: a polyester fibre (yellow) in galvanic contact with a grounded conductive stainless steel fibre (gray) are fixed on insulating double-face adhesive tape, a bias voltage V_{app} is applied to the AFM tip. (b) Measurement positions on the surface of the polyester fibre: P1 = cross point of the polyester fibre and the conductive fibre, P2 is 50 μm away from P1, P3 is 100 μm from P1 and P4 is 200 μm from P1). (For interpretation of the references to colour in this figure legend, the reader is referred to the Web version of this article.)

Charge electrification experiments were realized as follows. First, topographic and potential images of the polyester fibre surface were acquired in KPFM mode. Second, the AFM probe was brought into contact with the surface using the AFM contact mode with a controlled applied force (set point equal to ≈ 0.5 V). Third, a constant bias voltage, V_{app} = 10 or −10 V was applied to the probe during 60 s. Finally, topographic and surface potential images were acquired continuously to monitor the time variation of the surface potential on the charged spot.

The topographic and surface potential images were treated and analysed using home-made procedures developed on the Igor Pro software (WaveMetrics). From the successively acquired surface potential images, average profiles of the potential spots were obtained as 10 pixels wide profiles at the center of the image, allowing to obtain spot profiles at intervals of 256 s, the first profile corresponding to a time of 128 s. After subtraction of the background value of the surface potential, a gaussian function was used to fit the profiles and the following parameters were obtained: the peak height PH in volts and peak width W in μm. With these two parameters, the peak volume PV (V.μm^2) was estimated as follows

$$PV = \pi W^2 PH \quad (2)$$

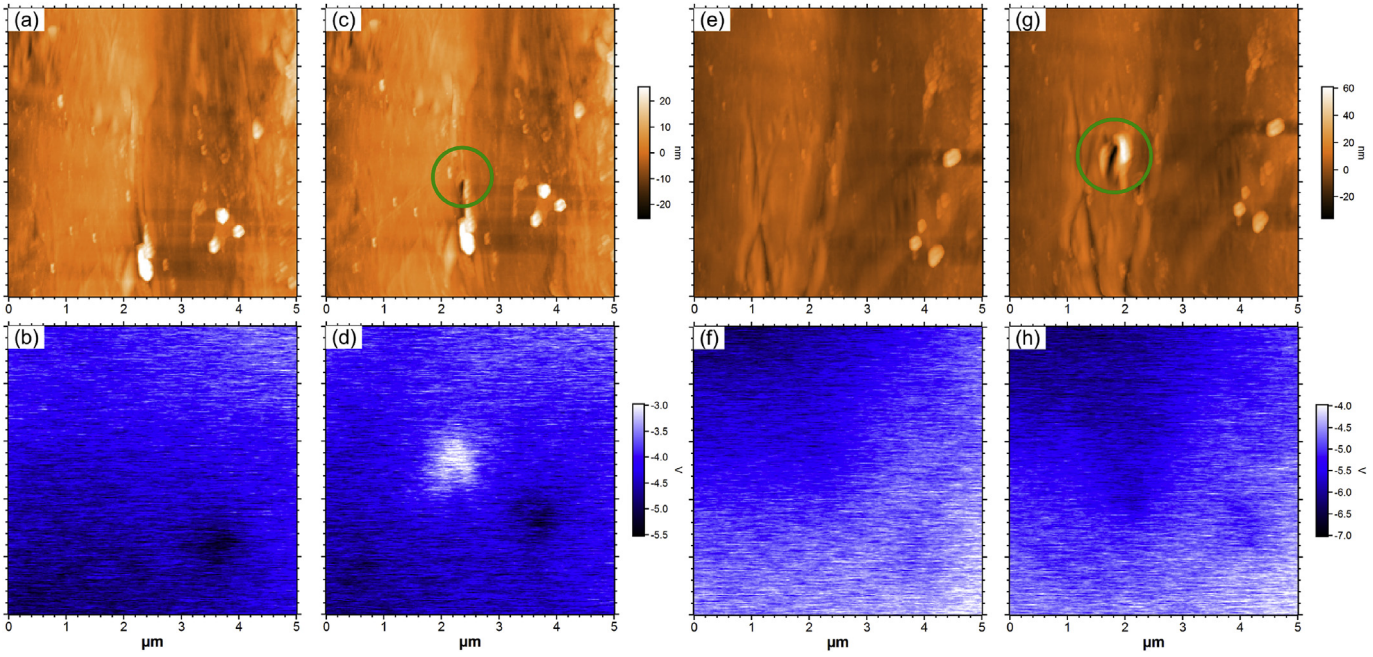

Fig. 2. Topography (a,c,e,g) and potential (b,d,f,h) images of charge spots deposited on polyester fibres with a bias voltage of +10 V (a,b,c,d) and of −10 V (e,f,g,h) at RH of 25%. (a,b,e,f) are the images obtained before the contact electrification and (c,d,g,h) are the images obtained just after contact electrification. Green circles mark the position where the tip was located during the charging. The bias was applied during 60 s. (For interpretation of the references to colour in this figure legend, the reader is referred to the Web version of this article.)

3. Results and discussion

3.1. Charge spot induction

Fig. 2 presents charge spots defined on the surface of a polyester fibre with positive (10 V) and negative (− 10 V) bias applied during 60 s. The indention marks left by the AFM probe (green circles) show the positions of the AFM tip during the contact electrification. On Fig. 2(d), the charge spot can be clearly observed and its position corresponds to the indentation position (Fig. 2(c)). For the negative bias, although the indentation clearly appears in the topographic image (Fig. 2(g)), no charge spot is clearly observed on the surface potential image (Fig. 2(h)). This suggests that different charging processes occur depending on the polarity of the charging tip.

In order to check that the generation of indentation marks did not influence the amount of deposited charges (charge spot height and width), the depth and width of the indentation marks were measured (see supplementary information). As can be seen in Table 1 in the supplementary information, no correlation between the charge spot parameters and the width and depth of the indentation marks was observed. This allowed to consider that the generation of indentation marks does not influence the amount of deposited charges and the size of the charge spots. This study also showed that the deposition of charges on different fibres under the same conditions of applied bias and relative humidity lead to the deposition of charge spots with similar values of peak height and width.

Fig. 2(b) and f shows that the contact potential between the Pt/Ir tip and the polyester fibre surface is negative and quite large. The average value of the contact potential is equal to − 4.3 V on Fig. 2(b) and to − 5.1 V on Fig. 2(f). This large negative value of the background contact potential explains why the measured surface potential may remain negative even after applying a large positive bias. This background contact potential had to be subtracted before analysing the charge spots as explained in the experimental section. Fig. 3 in the supplementary information presents potential images of charge spots calculated after subtracting the background contact potential.

Generally, we observed that the deposition of charge spots with negative bias voltages was more difficult and lacked of reproducibility. In order to check that this was not due to instrumental issues, charge deposition was also performed on a polystyrene (PS) film. Fig. 4 in the supplementary information shows that charge deposition with negative bias was possible on PS. This result can be first explained by considering the nature of the polymer, particularly the Lewis acidity, α, characterising the ability to accept electrons and the Lewis basicity, β, the tendency to give electrons. For polyester, Lewis acidity and Lewis basicity are equal to 0.54 and 0.66, respectively [41]. This means that polyester has a higher tendency to gives electrons than to accept electrons. This may explain why the deposition of charge spots with positive bias is easier than negative charging. A second reason may be that the large negative background contact potential make it difficult to observe negative charge spots. A third possibility is that the nature of the ionic species created at negative bias are more easily dispersed that the one generated at positive bias. It has been suggested in the literature that negatively charged ionic water clusters $[OH(H_2O)_n]^-$ could be the source of negative charging on polymers. These ionic clusters might not bind to polyester and might easily diffuse in the water contamination

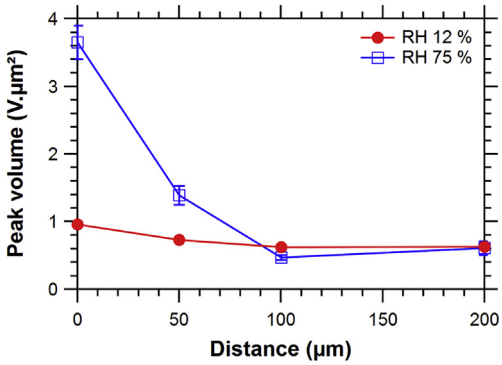

Fig. 3. Variation of the initial peak volume (after 128 s) as a function of the distance of the charging point from the crossing between the polyester fibre and the stainless steel fibre at the two extreme relative humidity values.

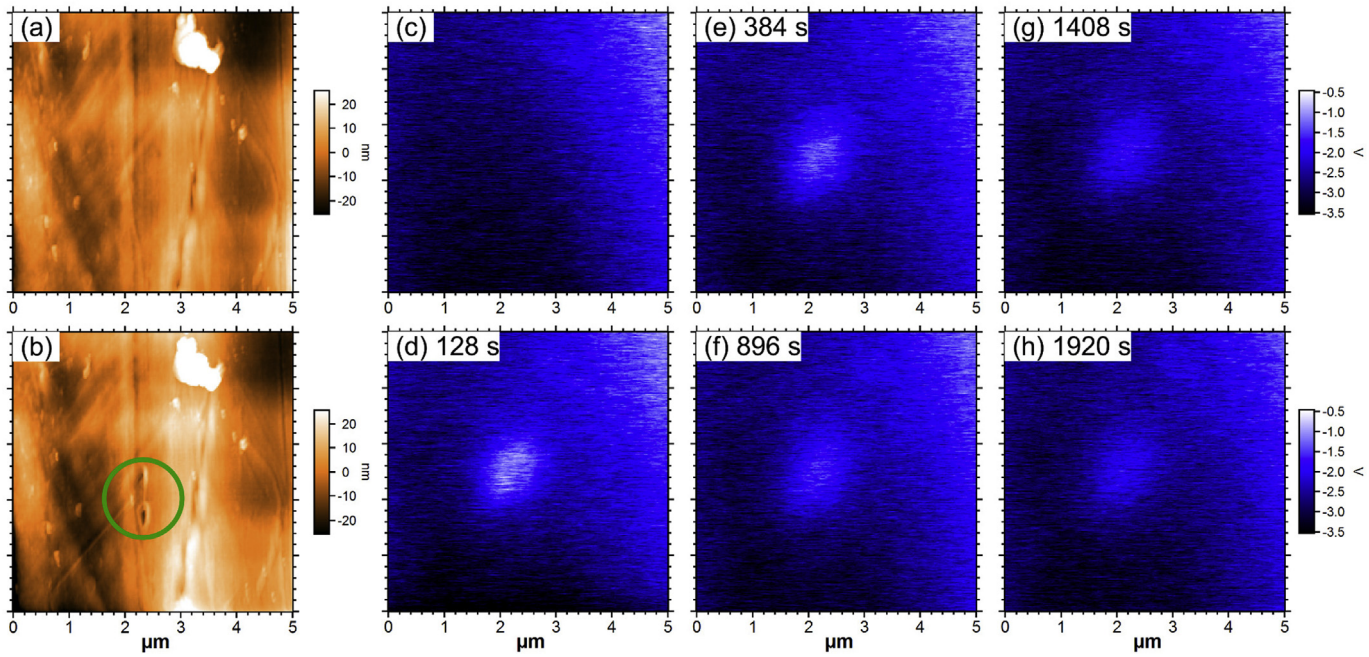

Fig. 4. Topography (a & b) and potential (c–h) images illustrating the dissipation of a charge spot deposited under 10 V (60 s) at 25% RH. (a & b) are the images before charge deposition; (c & d) are the images just after the charge deposition; (e to h) are successive potential images corresponding to different decay times (see insets). The green circle marks the position of the tip during the contact electrification. (For interpretation of the references to colour in this figure legend, the reader is referred to the Web version of this article.)

layer. In the remaining of this paper, only the results obtained with positive charging bias will be discussed.

The charge deposition process was investigated based on the values of the initial peak height, width and volume. The results were compared according to the contact distance and humidity conditions. Fig. 3 shows the variation of the initial peak volume for the different positions defined in Fig. 1 at the two extreme relative humidity conditions. The largest values of the peak volume are obtained at the cross point with the conductive fibre. The peak volume values are smaller at the other positions and remain almost constant with the distance from the cross point. The previously induced charge spots are not expected to affect the charging or discharging measurements at the next neighbouring point for two reasons. First, the distance between the different charging points along one fibre (~50 μm) was much larger than the width of the deposited charge spots (~1–2 μm). Second, it was possible to deposit isolated individual charge spots at much smaller distances, 1.5–2.5 μm (see Fig. 2 in the supplementary information).

As expected, it seems easier to perform surface charging just above the contact between the polyester fibre and the conductive fibre. This is consistent with the explanation given in the introduction [1]. Due to the large distance of the charging point with the conductive electrode, the deposited charges away from the contact point tend to accumulate on the other side of the fibre [21] and are thus not observed on the KPFM potential images. This charge diffusion may be eased by the humidity since the decrease of the peak volume with the distance from the contact point is more pronounced for 75% RH than for 12% RH. Therefore, to get the largest effect, all the remaining experiments were realized at the contact point with the conductive fibre.

From Fig. 3, it can also be observed that globally the volume of the initial charge spots reflecting the amount of deposited charges increases with the relative humidity. This behaviour may be explained by the fact that charge deposition is due to the field-adsorbed water meniscus mechanism. Ambient water can be field-adsorbed on the surface of the polyester fibre and dissociated near the biased probe ($6\,H_2O \rightarrow 4\,H_3O^+ + O_2 + 4\,e^-$). Positive ions may thus be injected on the surface of the polyester fibre.

3.2. Charge decay

Fig. 4 presents the results of a charge dissipation experiment on a polyester fibre at the cross-point with the conductive fibre after depositing a charge spot with a bias of 10 V during 60 s at 25% RH. The decrease of the surface potential on the charge spot after contact charging can be clearly observed on the potential images (Fig. 4(d–h)), corresponding to dissipation times of 128, 384, 896, 1408 and 1920 s, respectively. The charge spot measured after 128 s was always considered as the initial charge spot though some charges may already have disappeared.

The averaged surface potential profiles measured on the charge spots at selected times are presented in Fig. 5. As explained previously, the measured surface potential is related to the charge density; these results represent thus the evolution of the charge density as a function of time. On Fig. 5, gaussian fits of the spot profiles are also presented.

In Fig. 6, the time variations of the peak height, width and volume are compared for two different polyester fibres and for relative humidity values of 12 and 25%. Globally, the peak height decreases with

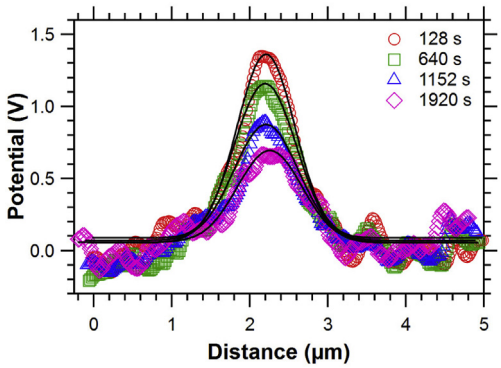

Fig. 5. Average surface potential profiles of charge spots extracted from the KPFM images after different decay times (see legend). Black curves are gaussian fits of the profiles.

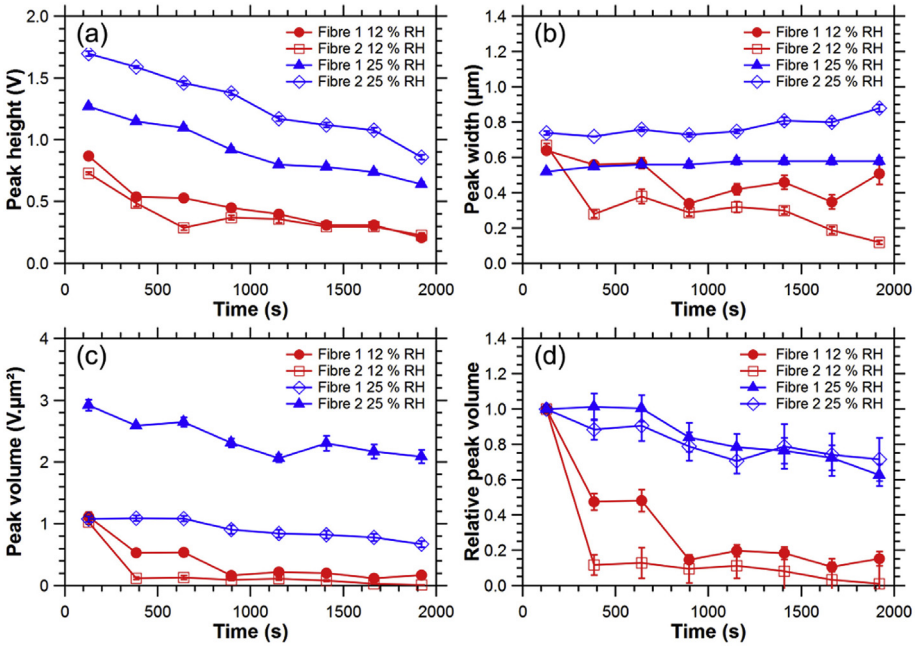

Fig. 6. Time dependence of peak height, peak width, peak volume and relative peak volume measured on two fibres at 12 and 25% RH.

time for both RH values. The peak width slightly decreases at 12% RH while it remains almost constant at 25% RH. As a result, the peak volume decreases with time in both cases.

In order to better compare the variations of the peak volume, the peak volume values were normalized by dividing them by the value of the peak volume after 128 s. The time variation of this relative peak volume is presented in Fig. 6(d). Similar behaviours are observed for both fibres for the same RH conditions. However, for the different RH conditions, different behaviours are observed. At 25% RH, the relative peak volume progressively decreases with time. At 12% RH, it first quickly decreases and then remains almost constant at a very low value.

Fig. 7(a and b) present surface potential images after contact electrification (10 V, 60 s) at the two extreme values of relative humidity, 12 and 75% respectively. Fig. 7(c,d,e) present the variation with time of the peak height, the peak width and the relative peak volume at the four studied RH values.

The potential images (Fig. 7(a and b)) show that fewer charges are initially deposited at 12% RH than at 75% RH. The analysis of the potential images obtained for the various values of RH after different times (Fig. 7(c–f)) show that different behaviours are observed depending on the RH.

Regarding the initial charge spots, the peak height is approximately the same for all the values of RH excepted for 25% RH where it is larger. Concerning the initial peak width the values are the same except for the charge spot deposited at 75% RH. Although the peak height of the initial charge spot observed at 75% RH after 128 s is small (Fig. 7(c)), a largest initial peak volume is observe, mainly due to the largest initial peak width (Fig. 7(d)).

The smaller peak height observed at 46 and 75% RH compared to that at 25% RH suggests that at 46 and 75% RH, a large amount of charges may already have been dissipated before 128 s. The hypothesis of fast charge dissipation at higher RH is supported by the fact that after 384 s, the charge spot almost disappeared (image not shown). In fact, the potential images obtained at the different values of RH showed that at 12 and 25% RH, charge spots remained observable even after 8 scans (2048 s) while at 46 and 75% RH, the charge spots almost fully disappeared after 4 scans (1152 s) (Fig. 7(c,d,e)).

Concerning the variation of the relative peak volume as a function of time (Fig. 7(e)), different behaviours are observed depending on the RH conditions. At 12% RH, the peak volume rapidly decreases from its small initial value to an even smaller value and then remains small and approximately constant on the time scale of the experiment. For 25% RH the peak volume decreases slightly and gradually and remains at a relatively high value within the time of the experiment. At 46 and 75% RH, the peak volume quickly decreases as for 12% RH but in these two cases the charge spots completely disappear after 4 scans, i.e. after 900 s. The peak width values follow almost the same trends. It remains almost constant at 25% RH, slightly decreases at 12% RH and quickly decreases at 46 and 75% RH.

Regarding contact electrification, the obtained results suggest that the field-adsorbed water meniscus mechanism is the dominant mechanism in the studied system. Larger relative humidity values lead to a thicker adsorbed water layer and hence a bigger meniscus around the tip. More hydronium cations may thus be generated and injected on the surface of the polyester fibre. This explanation is consistent with the observed global increase of the initial peak volume from 12 to 75% RH (Fig. 3).

In the literature, dissipation mechanisms are attributed to two main phenomenons: external dissipation via ion exchange with the close atmosphere and lateral dissipation or dissipation of the bulk material. External dissipation can be associated to water adsorption and desorption events. The surface carrying excess charges absorbs H_3O^+ ions for instance and exchange them with the atmosphere. Lateral diffusion dissipation implies charge transport in the dielectric towards the conductive support, perhaps also with concomitant neutralization with charges of opposite polarization. A simple model in terms of reaction-diffusion theory has been proposed for both modes of charge dissipation [33]. Since only positive charging is discussed here, the equation for positive charges is the following

$$\frac{\partial q^+}{\partial t} = D^+ \frac{\partial^2 q^+}{\partial x^2} - k_d^+ q^+ - k_n q^+ q^- \tag{3}$$

with q^+ and q^- the positive and negative charge densities respectively, D^+ the diffusion coefficient of positive charges, k_d^+ the external charge decay rate and k_n the rate of "fast" neutralization of charges with opposite polarization located at the same position. This model is based on the observation that charge transport in dielectrics is a diffusive mechanism [33]. If charge mobility is large, this equation predicts that the charge profiles should decay in magnitude while its width (area) broaden. This situation corresponds to charged patches becoming

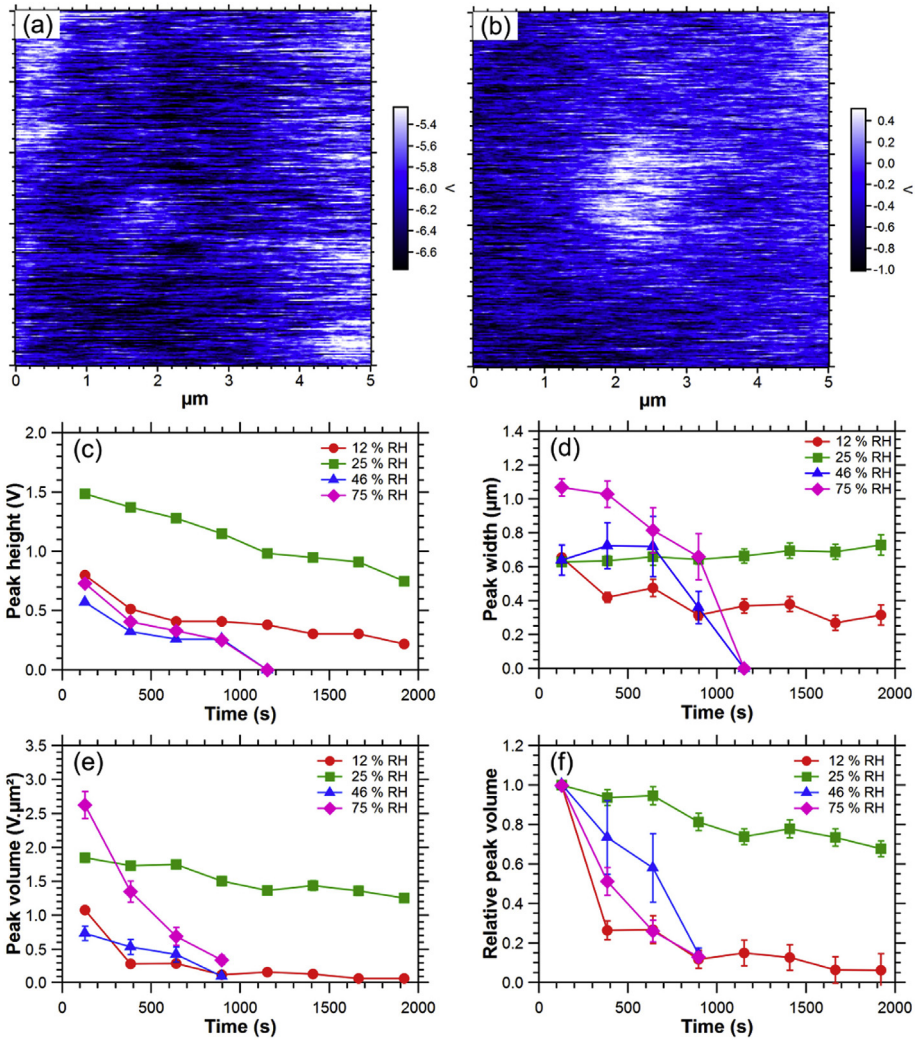

Fig. 7. Potential images after contact electrification (10 V, 60 s) at RH of (a) 12% and (b) 75%. Variation with time of (c) the peak height, (d) the peak width, (e) the peak volume and (f) the relative peak volume of charge spot at the four studied RH values.

blurry during the discharge process. On the other hand, if the lateral charge mobility is negligible, the charged area is expected to remain almost constant or to narrow.

According to the results obtained here, it may be inferred that the RH humidity strongly influences the dissipation of charge spots deposited on polyester fibres. First, charge dissipation appears to be greatly favoured by high relative humidity conditions as revealed by the dissipation curves (time dependence of the relative peak volume, Fig. 7(f)). The dissipation curve at 75% RH presents the largest slope corresponding to the fastest dissipation speed. Similarly, the dissipation curve at 46% RH also presents a fast decrease. In both cases, all the charges are dissipated after 1000 s. For 25 and 12% RH, the dissipation rates are slower. Second, it appears that charge dissipation for 12 and 25% RH occurs at almost constant charged area (Fig. 7(d)). In these two cases, lateral charge mobility seams to be negligible. The external dissipation mechanism is thus the main mechanism. For 46 and 75% RH, the charged areas tend to decrease (Fig. 7(d)) suggesting that in these two relative humidity conditions, the lateral dissipation mechanism may participate to charge dissipation along with the external dissipation mechanism.

It should be mentioned that the relative humidity not only influences the surface diffusion of the electrical charges on the polyester fibre surface but it also influences the water meniscus that is formed between the polyester fibre and the bottom contacting stainless steel fibre. The increase of relative humidity favours the formation of this water meniscus and will also favour electrical charge transfer between the polyester fibre surface and the stainless steel fibre.

4. Conclusions

Surface contact electrification experiments have been successfully performed with an AFM tip on the cylindrical surface of insulating polyester fibres in contact with a conductive fibre and the deposited charge spots have been characterised by KPFM as a function of time. The experimental procedure has been optimized in order to obtain clearly observable charge spots. With positive tip bias, charge spots have been deposited in a reproducible manner, the deposition of charges on different fibres under the same conditions of applied bias and relative humidity leading to the generation of similar charge spots. For negative tip bias, charges were hardly deposited. As a function of time, a decay of the deposited charge density was observed.

Based on the obtained results, the charging and charge dissipation mechanisms are discussed. For contact electrification, the result shows that the initial peak volume reflecting the amount of deposited charges increases with the increase of RH. This strongly indicates that the charge deposition is due to the field-adsorbed water meniscus mechanism.

Concerning the charge dissipation, two main mechanisms are identified and have different importance depending on the RH value. For 25 and 12% RH, the almost invariant charged areas suggest that

charge lateral mobility is negligible. The external dissipation mechanism, i.e. neutralization of the cations by anions present in the atmosphere and/or water meniscus, may thus be the main charge dissipation mechanism. For 46 and 75% RH, the charged areas tend to decrease. It thus suggests that the lateral diffusion mechanism and the external dissipation are both participating to charge dissipation. The increase of relative humidity will also favour charge dissipation by favouring the formation of the water meniscus between the polyester fibres and the stainless steel fibres.

Acknowledgements

The authors would like to thank Mr. B. Colson (Sioen Norcifa) for providing us with the Bekinox and polyester fibres. They also thank Prof. B. Vanderheyden (ULg), Prof. P. Vanderbemden (ULg) and Mr. Ph. Lemaire (Centexbel) for helpful discussions. This research was supported by FRIA (Fonds pour la formation à la Recherche dans lIndustie et dans lAgriculture) of F.R.S. - FNRS (Fonds de la Recherche Scientifique) and by the Belgian Federal Science Policy (IAP P6/27).

Appendix A. Supplementary data

Supplementary data to this article can be found online at https://doi.org/10.1016/j.elstat.2018.09.002.

References

[1] N. Gibson, Static electricity: an industrial hazard under control? J. Electrost. 40–41 (1997) 21–30, https://doi.org/10.1016/S0304-3886(97)00010-7.
[2] M. Glor, Electrostatic ignition hazards in the process industry, J. Electrost. 63 (2005) 447–453, https://doi.org/10.1016/j.elstat.2005.03.001.
[3] K. Tappura, S. Nurmi, Computational modeling of charge dissipation of fabrics containing conductive fibers, J. Electrost. 58 (2003) 117–133, https://doi.org/10.1016/S0304-3886(02)00202-4.
[4] A.G. Bailey, The charging of insulator surfaces, J. Electrost. 51–52 (2001) 82–90, https://doi.org/10.1016/S0304-3886(01)00106-1.
[5] J. Chubb, Measurement of charge transfer in electrostatic discharges, J. Electrost. 64 (2006) 321–325, https://doi.org/10.1016/j.elstat.2005.08.003.
[6] J. Mi, S. Du, G. Yuan, Study on both discharge and charging of the earthed atomizing corona discharge and the influence of magnetic fields on them, Curr. Appl. Phys. 12 (2012) 1005–1010, https://doi.org/10.1016/j.cap.2011.11.019.
[7] P. Kathirgamanathan, M.J. Toohey, J. Haase, P. Holdstock, J. Laperre, G. Schmeer-Lioe, Measurements of incendivity of electrostatic discharges from textiles used in personal protective clothing, J. Electrost. 49 (2000) 51–70, https://doi.org/10.1016/S0304-3886(00)00003-6.
[8] H. Salmela, J. Paasi, T. Kalliohaka, L. Fast, Measurements of air discharges from insulating, electrostatic dissipative and conductive materials with different ESD probes, J. Electrost. 63 (2005) 539–544, https://doi.org/10.1016/j.elstat.2005.03.025.
[9] M. Boutaayamou, P. Lemaire, B. Vanderheyden, P. Vanderbemden, Design and fabrication of an electrode array sensor for probing the electric potential distribution at the mesoscopic scale in antistatic felts, Meas. Sci. Technol. 25 (2014) 075903, https://doi.org/10.1088/0957-0233/25/7/075903.
[10] T. Kalliohaka, J. Paasi, P. Lemaire, Forced corona method for the evaluation of fabrics with conductive fibres, J. Electrost. 63 (2005) 583–588, https://doi.org/10.1016/j.elstat.2005.03.020.
[11] G. Chen, A new model for surface potential decay of corona-charged polymers, J. Phys. D Appl. Phys. 43 (2010) 055405, https://doi.org/10.1088/0022-3727/43/5/055405.
[12] L. Herous, M. Remadnia, M. Kachi, M. Nemamcha, Decay of electrical charges on polyethylene terephthalate surface, J. Eng. Sci. Technol. Rev. 2 (2009) 87–90.
[13] N. Cornet, D. Goeuriot, C. Guerret-Piécourt, D. Juvé, D. Tréheux, M. Touzin, H.-J. Fitting, Electron beam charging of insulators with surface layer and leakage currents, J. Appl. Phys. 103 (2008) 064110, https://doi.org/10.1063/1.2890427.
[14] M. Touzin, D. Goeuriot, C. Guerret-Piécourt, D. Juvé, D. Tréheux, H.-J. Fitting, Electron beam charging of insulators: a self-consistent flight-drift model, J. Appl. Phys. 99 (2006) 114110, https://doi.org/10.1063/1.2201851.
[15] M. Kotera, Y. Matsumoto, Time dependent charging of insulators by electron beam irradiation, Microsc. Microanal. 11 (2005) 1690–1691, https://doi.org/10.1017/s1431927605504379.
[16] T.A.L. Burgo, T.R.D. Ducati, K.R. Francisco, K.J. Clinckspoor, F. Galembeck, S.E. Galembeck, Triboelectricity: macroscopic charge patterns formed by self-arraying ions on polymer surfaces, Langmuir 28 (2012) 7407–7416, https://doi.org/10.1021/la301228j.
[17] T.A.L. Burgo, A. Erdemir, Bipolar tribocharging signal during friction force fluctuations at metal-insulator interfaces, Angew. Chem. Int. Ed. 53 (2014) 12101–12105, https://doi.org/10.1002/anie.201406541.
[18] L.C. Soares, S. Bertazzo, T.A.L. Burgo, V. Baldim, F. Galembeck, A new mechanism for the electrostatic charge build-up and dissipation in dielectrics, J. Braz. Chem. Soc. 19 (2008) 277–286.
[19] S. Cunningham, Dynamical studies of the single point contact electrification of inorganic and polymer substrates, J. Electrost. 40–41 (1997) 225–230.
[20] G.S.P. Castle, L.B. Schein, General model of sphere-sphere insulator contact electrification, J. Electrost. 36 (1995) 165–173.
[21] C.A. Rezende, R.F. Gouveia, M.A. da Silva, F. Galembeck, Detection of charge distributions in insulator surfaces, J. Phys. Condens. Matter 21 (2009) 263002, https://doi.org/10.1088/0953-8984/21/26/263002.
[22] M. Nonnenmacher, M.P. O'Boyle, H.K. Wickramasinghe, Kelvin probe force microscopy, Appl. Phys. Lett. 58 (1991) 2921, https://doi.org/10.1063/1.105227.
[23] W. Melitz, J. Shen, A.C. Kummel, S. Lee, Kelvin probe force microscopy and its application, Surf. Sci. Rep. 66 (2011) 1–27, https://doi.org/10.1016/j.surfrep.2010.10.001.
[24] V. Palermo, M. Palma, P. Samorì, Electronic characterization of organic thin films by kelvin probe force microscopy, Adv. Mater. 18 (2006) 145–164, https://doi.org/10.1002/adma.200501394.
[25] N. Afsharimani, B. Nysten, Electronic properties of dioctylterthiophene-based organic thin-film transistors: a kelvin probe force microscopy study, Thin Solid Films 536 (2013) 295–301, https://doi.org/10.1016/j.tsf.2013.04.010.
[26] R. Berger, H.-J. Butt, M.B. Retschke, S.A.L. Weber, Electrical modes in scanning probe microscopy, Macromol. Rapid Commun. 30 (2009) 1167–1178, https://doi.org/10.1002/marc.200900220.
[27] C. Lian, H.G. Xing, Surface potential measurements on ni-(al)gan lateral Schottky junction using scanning kelvin probe microscopy, Appl. Phys. Lett. 88 (2006) 022112, https://doi.org/10.1063/1.2163073.
[28] Y.S. Zhou, S. Wang, Y. Yang, G. Zhu, S. Niu, Z.-H. Lin, Y. Liu, Manipulating nanoscale contact electrification by an applied electric field, Nano Lett. 14 (2014) 1567–1572, https://doi.org/10.1021/nl404819w.
[29] B. Terris, J. Stern, D. Rugar, H. Mamin, Contact electrification using force microscopy, Phys. Rev. Lett. 63 (1989) 2669–2672, https://doi.org/10.1103/PhysRevLett.63.2669.
[30] N. Knorr, S. Vinzelberg, Charge writing and detection by efm and kpfm scanning probe techniques, Microsc. Anal. 26 (2012) 6.
[31] S. Morita, Y. Sugawara, Microscopic contact charging and dissipation, Thin Solid Films 393 (2001) 310–318, https://doi.org/10.1016/S0040-6090(01)01102-6.
[32] R.F. Gouveia, C.A.R. Costa, F. Galembeck, Electrostatic patterning of a silica surface: a new model for charge build-up on a dielectric solid, J. Phys. Chem. B 109 (2005) 4631–4637, https://doi.org/10.1021/jp0457601.
[33] H.T. Baytekin, A.Z. Patashinski, M. Branicki, B. Baytekin, S. Soh, B.A. Grzybowski, The mosaic of surface charge in contact electrification, Science 333 (2011) 308–312, https://doi.org/10.1126/science.1201512.
[34] S. Cunningham, I.A. Larkin, J.H. Davis, Noncontact scanning probe microscope potentiometry of surface charge patches: origin and interpretation of time-dependent signals, Appl. Phys. Lett. 73 (1998) 123–125, https://doi.org/10.1063/1.121788.
[35] A. Belarni, M. Lamhamdi, P. Pons, L. Boudou, J. Guastavino, Y. Segui, Kelvin probe microscopy for reliability investigation of rf- mems capacitive switches, Microelectron. Reliab. 48 (2008) 1232–1236.
[36] M. Ishii, Static states and dynamic behaviour of charges: observation and control by scanning probe microscopy, J. Phys. Condens. Matter 22 (2010) 173001, https://doi.org/10.1088/0953-8984/22/17/173001.
[37] N. Knorr, R. Wirtz, S. Rosselli, G. Nelles, Field-absorbed water and induced electrochemical and processes in organic and thin film and junctions, J. Phys. Chem. C 114 (2010) 15791–15796, https://doi.org/10.1021/jp103625w.
[38] H.T. Baytekin, B. Baytekin, J.T. Incorvati, B.A. Grzybowski, Material transfer and polarity reversal in contact charging, Angew. Chem. Int. Ed. 51 (2012) 4843–4847, https://doi.org/10.1002/anie.201200057.
[39] S. Magonov, J. Alexander, Single-pass kelvin force microscopy and dc/dz measurements in the intermittent contact: applications to polymer materials, Beilstein J. Nanotechnol. 2 (2011) 15–27, https://doi.org/10.3762/bjnano.2.2.
[40] J. Yin, C. D'Haese, B. Nysten, Surface electrical properties of stainless steel fibres: an afm-based study, Appl. Surf. Sci. (2015) 65–73, https://doi.org/10.1016/j.apsusc.2014.12.188.
[41] A.F. Diaz, R.M. Felix-Navarro, A semi-quantitative tribo-electric series for polymeric materials: the influence of chemical structure and properties, J. Electrost. 62 (2004) 277–290, https://doi.org/10.1016/j.elstat.2004.05.005.